PLAXIS

essential for geotechnical professionals

PLAXIS

Thermal and coupled THM analysis

2015

Plaxis bv P.O. Box 572, 2600 AN DELFT, Netherlands

Fax: +31 (0)15 257 3107; E-mail: info@plaxis.nl; Internet site: www.plaxis.nl

Printed in the Netherlands

TABLE OF CONTENTS

1 FEATURES AND LIMITATIONS

The Thermal add-on module with PLAXIS 2D implements several new features:

- THM couplings for unsaturated soils
- Fully coupled formulation and implementation
- Availability of temperature for User Defined Soil Models (UDSM)
- Ground freezing
- Vapour flux
- Anisotropic thermal expansion
- Effect of temperature on permeability
- Convective boundary conditions
- Freeze pipes
- Enhanced post processing

Limitations:

- No effect of temperature on the retention curve and on mechanical properties.

2 GOVERNING EQUATIONS

In this section the governing equations of fully coupled thermo-hydro-mechanical analysis are briefly described. This is an extension to the implementation of fully coupled hydro-mechanical analysis (flow-deformation). Here, non-isothermal unsaturated groundwater flow, heat transport and deformation are considered. Similar to the previous work, we assume a constant gas pressure. Therefore, only one independent unknown in the fluid mass balance equation is needed which is pore water pressure. This study is based on the assumption of local thermodynamic equilibrium which means that all phases have the same temperature. Therefore only one equation of total energy is required. Therefore the new variables are displacements (v), pore water pressure (p_w) and temperature (T).

2.1 NON ISOTHERMAL UNSATURATED WATER FLOW

An extended Richard's model is applied to describe non isothermal unsaturated flow. The mass flux of water is defined as:

$$\underline{J}_w = \rho_w \left(\frac{k_{rel}}{\mu} \underline{\underline{\kappa}}^{int} (\nabla p_w + \rho_w \underline{g}) \right) \tag{2.1}$$

where μ is the dynamic viscosity of the fluid and $\underline{\underline{\kappa}}^{int}$ is the intrinsic permeability of the porous medium. The dynamic viscosity depends on the type of fluid and temperature and the intrinsic permeability is a function of porous structure. In an unsaturated state the coefficient of permeability depends on the soil saturation. The relative permeability $k_{rel}(S)$ is defined as the ratio of the permeability at a given saturation to the permeability in saturated state. $\underline{g} = (0, -g, 0)^T$ is the vector of gravitational acceleration. n and S are porosity and degree of saturation, respectively.

Due to the effects of temperature, vapour flow effects need to be considered in a non-isothermal processes. The mass flux of vapour is defined as Rutqvist, Borgesson, Chijmatsu, Kobayashi, Jing, Nguyen, Noorishad & Tsang (2001)

$$\underline{J}_v = -D_v \nabla \rho_v = D_{pv} \nabla p_w - D_{Tv} \nabla T \tag{2.2}$$

where T is local equilibrium temperature of the porous medium in Kelvin. D_{pv} and D_{Tv} are hydraulic and thermal diffusion coefficients:

$$D_{pv} = D_v \left(\frac{\partial \rho_v}{\partial p_w} \right) = \frac{D_v \rho_v}{\rho_w RT} \tag{2.3}$$

$$D_{Tv} = f_{Tv} D_v \left(\frac{\partial \rho_v}{\partial T} \right) = f_{Tv} D_v \left(\theta \frac{\partial \rho_{vS}}{\partial T} + \frac{\rho_v p_w}{\rho_w RT^2} \right) \tag{2.4}$$

D_v is the vapour diffusion coefficient in a porous material which depends on temperature, gas pressure, medium tortuousity and gas pressure. f_{Tv} is the thermal diffusion enhancement factor. ρ_v is the vapour density and ρ_{vS} is the saturated vapour density

which is the density of vapour at phreatic level. The relative humidity θ is defined as:

$$\theta = exp\left(\frac{-p_w}{\rho_w RT}\right) \tag{2.5}$$

where R is the specific gas constant for water vapour. The vapour density ρ_v is related to the temperature dependent saturated vapour density by Rutqvist, Borgesson, Chijmatsu, Kobayashi, Jing, Nguyen, Noorishad & Tsang (2001)

$$\rho_v = \theta \rho_{vS} \tag{2.6}$$

The saturated vapour density is a function of temperature only. It can be obtained from empirical relationships published in the literature. Here an empirical function published in Wang, Kosakowski & Kolditz (2009) is adopted:

$$\rho_{vS} = 10^{-3} exp\left(19.891 - \frac{4974}{T}\right) \tag{2.7}$$

in which ρ_{vS} is in kg/m^3 and T in Kelvin.

2.2 MASS BALANCE EQUATION

The water mass balance can be written in the following form Rutqvist, Borgesson, Chijmatsu, Kobayashi, Jing, Nguyen, Noorishad & Tsang (2001):

$$n\frac{\partial}{\partial t}(S\rho_w+(1-S)\rho_v)+(S\rho_w+(1-S)\rho_v)\left[\frac{\partial \varepsilon_v}{\partial t}+\frac{1-n}{\rho_s}\frac{\partial \rho_s}{\partial t}\right] = -\nabla\cdot(\underline{J}_w+\underline{J}_v) \tag{2.8}$$

The first term of the left-hand side can be expanded as:

$$\begin{aligned} n\frac{\partial}{\partial t}(S\rho_w + (1-S)\rho_v) &= n\frac{\partial S}{\partial t}\rho_w + nS\frac{\partial \rho_w}{\partial t} - n\frac{\partial S}{\partial t}\rho_v + n(1-S)\frac{\partial \rho_v}{\partial t} \\ &= n\left(\frac{\partial S}{\partial p_w}\frac{\partial p_w}{\partial t}+\frac{\partial S}{\partial T}\frac{\partial T}{\partial t}\right)\rho_w \\ &\quad +nS\left(-\rho_w\alpha_{wP}\frac{\partial p_w}{\partial t}-\rho_w\alpha_{wT}\frac{\partial T}{\partial t}\right) \\ &\quad -n\left(\frac{\partial S}{\partial p_w}\frac{\partial p_w}{\partial t}+\frac{\partial S}{\partial T}\frac{\partial T}{\partial t}\right)\rho_v \\ &\quad +n(1-S)\rho_w\left[\frac{\rho_v}{\rho_w^2 R_v T}\frac{\partial p_w}{\partial t}+\left(\frac{\theta}{\rho_w}\frac{\partial \rho_{vS}}{\partial T}+\frac{\rho_v p_w}{\rho_w^2 R_v T^2}\right)\frac{\partial T}{\partial t}\right] \end{aligned} \tag{2.9}$$

where α_{wP} and α_{wT} are the compressibility and volumetric thermal expansion of water. The volumetric thermal expansion of water at 293.15 K is $2.1.10^{-4}$. The water density is related to the water pressure and temperature through:

$$\frac{\rho_w}{\rho_{w0}} = 1-\alpha_{wP}(p_w-p_{w0})-\alpha_{wT}(T-T_0) \tag{2.10}$$

The second term of the left-hand side of Eq. (2.8) can be expanded as:

$$
\begin{aligned}
&(S\rho_w + (1-S)\rho_v)\left[\frac{\partial \varepsilon_v}{\partial t} + \frac{1-n}{\rho_s}\frac{\partial \rho_s}{\partial t}\right] \\
&= (S\rho_w + (1-S)\rho_v)\left[\frac{\partial \varepsilon_v}{\partial t} - (1-n)\alpha_{sT}\frac{\partial T}{\partial t}\right] \\
&= (S\rho_w + (1-S)\rho_v)\frac{\partial \varepsilon_v}{\partial t} - (S\rho_w + (1-S)\rho_v)(1-n)\alpha_{sT}\frac{\partial T}{\partial t}
\end{aligned}
\tag{2.11}
$$

where α_{sT} is the volumetric thermal expansion of soil grains. By substituting Eq. (2.11) and Eq. (2.9) into Eq. (2.8), the water mass balance can be derived as:

$$
\begin{aligned}
&\left[n(\rho_w - \rho_v)\frac{\partial S}{\partial p_w} - nS\rho_w\alpha_{wP0} - n(1-S)\frac{\rho_v}{\rho_w R_v T}\right]\frac{\partial p_w}{\partial t} \\
&\quad + \left[n(\rho_w - \rho_v)\frac{\partial S}{\partial T} - nS\rho_w\alpha_{wT0} - n(1-S\right) \\
&\quad \left(\theta\frac{\partial \rho_{vS}}{\partial T} + \frac{\rho_v p_w}{\rho_w R_v T^2}\right) \\
&\quad - (S\rho_w + (1-S)\rho_v)(1-n)\alpha_{sT}]\frac{\partial T}{\partial t} \\
&\quad + (S\rho_w + (1-S)\rho_v)\frac{\partial \varepsilon_v}{\partial t} + \nabla\cdot(\underline{J}_w + \underline{J}_v) = 0
\end{aligned}
\tag{2.12}
$$

It should be noted that the term $(1-S)\rho_v$ can be neglected for saturated state and low temperature in comparison with $S\rho_w$. However, in the case of very dry and high temperature, this term may be significant.

2.3 NON-ISOTHERMAL DEFORMATION

For a representative elemental volume of the soil the linear momentum balance is given by:

$$\nabla\cdot\underline{\underline{\sigma}} + \rho\underline{g} = 0 \tag{2.13}$$

where

$$\rho = (1-n)\rho_s + nS\rho_w + n(1-S)\rho_g \tag{2.14}$$

is the multiphase medium. ρ_s, ρ_w and ρ_g are the solid, water and gas densities. $\underline{g}$ is a vector containing the gravity acceleration: $\underline{g}^T = (0, -g, 0)^T$ in the 3D space. In Eq. (2.13), $\underline{\underline{\sigma}}$ is the total stress. For partially saturated soils the total stress can be written in the following form:

$$\underline{\underline{\sigma}} = \underline{\underline{\sigma}}' + P\underline{\underline{m}} \tag{2.15}$$

where $\underline{\underline{m}}$ is the identity tensor, $\underline{\underline{\sigma}}'$ is the effective stress and P is the average pore pressure, which is a function of the pore water pressure, the pore gas pressure the degree of saturation of water and the degree of saturation of gas:

$$P = S_w P_w + S_g P_g = Sp_w + (1-S)p_g \tag{2.16}$$

By substituting the average pore pressure into Eq. (2.15) we have:

$$\underline{\underline{\sigma}} = \underline{\underline{\sigma}}' + (Sp_w + (1 - S)p_g)\underline{\underline{m}} \tag{2.17}$$

If the degree of saturation is replaced by the matric suction coefficient χ, the well known Bishop's stress (average stress) is obtained:

$$\underline{\underline{\sigma}} = \underline{\underline{\sigma}}' + (\chi p_w + (1 - \chi)p_g)\underline{\underline{m}} \tag{2.18}$$

χ is an experimentally determined factor which depends on degree of saturation, porosity, and the matric suction. As the pore gas pressure is assumed to be constant and equal to the atmospheric pressure, the pore gas pressure can be neglected. Therefore the Bishop's stress can be simplified as:

$$\underline{\underline{\sigma}} = \underline{\underline{\sigma}}' + \chi p_w \underline{\underline{m}} \tag{2.19}$$

The constitutive relation using the effective stress $\underline{\underline{\sigma}}'$ is written in the following form:

$$d\underline{\underline{\sigma}}' = \underline{\underline{M}} : (d\underline{\underline{\varepsilon}} - d\underline{\underline{\varepsilon}}_T) \tag{2.20}$$

$\underline{\underline{M}}$ represents the material stress-strain matrix. $\underline{\underline{\varepsilon}}$ is the total strain of the skeleton and $\underline{\underline{\varepsilon}}_T$ is thermal strain caused by temperature increase. The thermal strain can be found from:

$$d\underline{\underline{\varepsilon}}_T = \underline{\underline{B}}_{DT}\underline{\underline{m}}\, dT = \begin{bmatrix} \alpha_{DT,x} & 0 & 0 & 0 & 0 & 0 \\ 0 & \alpha_{DT,y} & 0 & 0 & 0 & 0 \\ 0 & 0 & \alpha_{DT,z} & 0 & 0 & 0 \\ 0 & 0 & 0 & 0 & 0 & 0 \\ 0 & 0 & 0 & 0 & 0 & 0 \\ 0 & 0 & 0 & 0 & 0 & 0 \end{bmatrix} \underline{\underline{m}}\, dT$$

where $\alpha_{DT,x}$, $\alpha_{DT,y}$ and $\alpha_{DT,z}$ are the drained linear thermal expansion coefficient of soil skeleton K^{-1} in x, y and z directions, respectively, which vary between $0.5\,10^{-6}$ and $12\,10^{-6}K^{-1}$ depending on the type of the soil or rock. Khalili, Uchaipichat & Javadi (2010) showed that the thermal expansion coefficient of soils grains is the same as the skeletal thermal expansion coefficient of homogeneous porous media. Therefore

$$\alpha_{sT} = \alpha_{DT,x} + \alpha_{DT,y} + \alpha_{DT,z} \tag{2.21}$$

Therefore the constitutive relation can be written as:

$$d\underline{\underline{\sigma}}' = \underline{\underline{M}} : (d\underline{\underline{\varepsilon}} - \underline{\underline{B}}_{DT}\underline{\underline{m}}\, dT) \tag{2.22}$$

The governing equation for the deformation model is obtained:

$$\nabla \cdot \left[\underline{\underline{M}} : (d\underline{\underline{\varepsilon}} - \underline{\underline{B}}_{DT}\underline{\underline{m}}\, dT) + \chi d p_w \underline{\underline{m}}\right] + d(\rho \underline{g}) = 0 \tag{2.23}$$

2.4 HEAT TRANSPORT

The heat balance equation for the porous medium can be written in the following form:

$$\frac{\partial}{\partial t}(nS\rho_w e_w + n(1-S)\rho_v e_v + (1-n)\rho_s e_s) = -\nabla \cdot (\underline{J}_w + \underline{J}_v) + Q_T \tag{2.24}$$

in which e_w, e_v and e_s are the internal energy in the water, vapour and solid phases, respectively. Q_T is the heat source term, i.e. heat generation rate per unit volume. $\underline{J}_{Aw}$ and $\underline{J}_c$ are the advective internal energy flux in water and the conductive (diffusive) heat flux in the porous medium, respectively. The conductive heat flow is assumed to be governed by Fourier's law:

$$\underline{J}_c = -\lambda \nabla T \tag{2.25}$$

where λ is the thermal conductivity of the porous medium:

$$\lambda = (1-n)\lambda_s + nS\lambda_w + n(1-S)\lambda_g \tag{2.26}$$

λ_s, λ_w and λ_g are the solid, the water and the gas thermal conductivities. The advective internal energy flux in water is:

$$\underline{J}_{Aw} = C_w T \underline{J}_w = \rho_w C_w T \left(\frac{k_{rel}}{\mu} \underline{\underline{\kappa}}^{int} (\nabla p_w + \rho_w \underline{g}) \right) = \rho_w C_w \underline{V}_w T \tag{2.27}$$

in which $\underline{V}_w$ is the water phase velocity and C_w is the water specific heat capacity. The total heat flux in an unsaturated porous medium is a summation of diffusive heat flux and advective flux:

$$\underline{J}_T = \underline{J}_c + \underline{J}_{Aw} - \lambda \nabla T + \rho_w C_w \underline{V}_w T \tag{2.28}$$

The mechanical energy conversions in fluid and solid phases are included in the source term:

$$Q_T = \underline{\underline{\sigma}}_w : \nabla \underline{V}_w + \underline{\underline{\sigma}}_s : \nabla \underline{V}_s = (nS_w p_w \nabla \cdot \underline{V}_w - \tau_w) + (1-n)\, 3K\prime \alpha_{DT} \frac{\partial \varepsilon_v}{\partial t} \tag{2.29}$$

where $\underline{\underline{\sigma}}_w$ and $\underline{\underline{\sigma}}_s$ are the stress tensor in the water and solid phases, respectively. $\underline{V}_s$ is the solid phase velocity and τ_w is a viscous energy dissipation term. The source term Q_T is an internal/external supply which can be neglected in most practical applications. The left hand side of the heat balance equation (the heat storage term) can be simplified as:

$$\frac{\partial}{\partial t}(nS\rho_w e_w + n(1-S)\rho_v e_v + (1-n)\rho_s e_s) = \rho C \frac{\partial T}{\partial t} \tag{2.30}$$

where ρC is the heat capacity of the porous medium:

$$\rho C = (1-n)\rho_s C_s + nS\rho_w C_w + n(1-S)\rho_v C_v \tag{2.31}$$

C_s, C_w and C_c are the solid, the water and the gas specific heat capacities. The right hand side of the heat balance equation can be expanded as:

$$\nabla \cdot \underline{J}_T = \nabla \cdot \underline{J}_c + \nabla \cdot \underline{J}_{Aw} = -\nabla \cdot (\lambda \nabla T) + \nabla \cdot (\rho_w C_w \underline{V}_w T) \tag{2.32}$$

in which

$$\nabla \cdot (\rho_w C_w \underline{V}_w T) = nS\rho_w C_w (\underline{V}_w \cdot \nabla T + T\nabla \cdot \underline{V}_w)$$
$$= \rho_w C_w \left[\frac{k_{rel}}{\mu} \underline{\underline{\kappa}}^{int} (\nabla p_w + \rho_w \underline{g}) \right] \cdot \nabla T + \rho_w C_w T \left[\nabla \cdot \left(\frac{k_{rel}}{\mu} \underline{\underline{\kappa}}^{int} (\nabla p_w + \rho_w \underline{g}) \right) \right] \quad (2.33)$$

The governing equation on heat transport can therefore be written as:

$$\rho C \frac{\partial T}{\partial t} - \nabla \cdot (\lambda \nabla T) \left[\frac{k_{rel}}{\mu} \underline{\underline{\kappa}}^{int} (\nabla p_w + \rho_w \underline{g}) \right] \cdot \nabla T + \rho_w C_w T \left[\nabla \cdot \left(\frac{k_{rel}}{\mu} \underline{\underline{\kappa}}^{int} (\nabla p_w + \rho_w \underline{g}) \right) \right] - Q_T - C_{as}(T - T_a) = 0 \quad (2.34)$$

T_a is the air temperature and C_{as} (W/m^2K) is the convective heat transfer coefficient at the surface in contact with air.

2.5 SOIL FREEZING

Below $0° C$, liquid water turns into ice. This phase change is taken into account via a modification in the storage term: additional energy has to be provided. This energy depends on the latent heat of water and on the evolution of the unfrozen water content with respect to temperature. The unfrozen water content is the amount of liquid water in the pores that has not been converted into ice. Figure 2.1 shows the evolution of the unfrozen water content w_u with respect to temperature for several soils:

The heat capacity Eq. (2.31) then becomes:

$$\rho C = (1 - n)\rho_s C_s + nS\rho_w \left(C_w + l \frac{dw_u}{dT} \right) + n(1 - S)\rho_v C_v \quad (2.35)$$

where l is the latent heat of liquid water. The function $w_u(T)$ is defined by the user using a table, as it is material dependent. The thermal conductivity is also modified to reflect the formation of ice:

$$\lambda = (1 - n)\lambda_s + nS[w_u \lambda_w + (1 - w_u)\lambda_i] + n(1 - S)\lambda_g \quad (2.36)$$

where λ_i is the thermal conductivity of the ice.

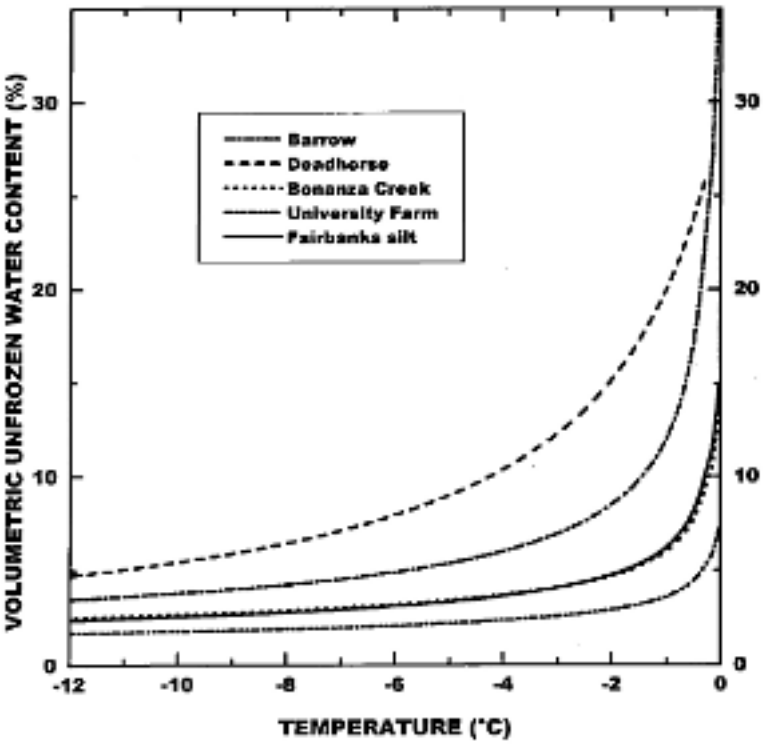

Figure 2.1 Influence of temperature on unfrozen water content for different soils (Romanovsky & Osterkamp (2000))

3 BOUNDARY CONDITIONS

Four types of boundary conditions are available:

- Dirichlet
- Neumann
- Convection
- Freezing pipe

Dirichlet means imposed temperature, on a line or on a cluster. Neumann means that a flux is prescribed: inflow or outflow. A closed boundary condition is a Neumann boundary condition with a null flux.

Convective boundary conditions are defined following equation (Eq. (3.1)):

$$Q = R(T - T_{fluid}) \tag{3.1}$$

In this equation, T is the temperature of the system, T_{fluid} is the temperature of the fluid in contact with the boundary, and R is an amplitude coefficient, like a resistivity. The efficiency of such a boundary condition depends on the resistivity. A infinite resistivity corresponds to a Dirichlet boundary condition (i.e. no loss of heat), while a small resistivity can be used to model insulation. Freezing pipes are based on the convective boundary condition and follow the same formulation.

4 VALIDATION: ONE-DIMENSIONAL HEAT FLOW

4.1 SOIL ELEMENTS

Thorough validation of thermo-hydro-mechanical couplings is difficult due to the number of phenomena involved. These many interactions limit the possibilities of analytical validations. Validation against experimental data is under process. Results will be added to this manual as soon as satisfactory studies are completed.

Analytical solutions are available for non porous materials, i.e. thermo-mechanical couplings. The purpose of the following study is to provide a set of simple tests to check the behaviour of the implementation. To do so, a general framework is set. It consists of two samples, for 1D and 2D, to which are applied different boundary conditions. This will allow better understanding and checking of the results.

For each test case, transient and steady state flows are considered. At the time of writing, the steady state for thermal flow is obtained after the transient period. For each test case, all the types of boundary conditions are tested, both independently and coupled.

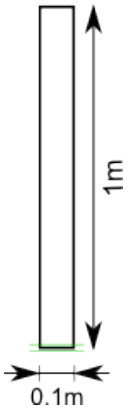

Figure 4.1 Geometry used for 1D tests

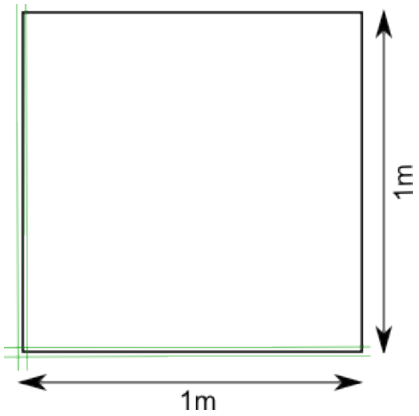

Figure 4.2 Geometry used for 2D tests, in both plain strains and axisymetric cases

The geometries of the studied samples are shown at Figure 4.1 for 1D and Figure 4.2 for 2D. The purpose of this chapter is to test the implementation when considering the soil as a continuous material. There are two ways to do so in PLAXIS set the material as non porous and set its cluster to dry. In the following, both cases are considered for each test, but they will not be commented if the results are the same.

To simplify the reading of this study, a naming convention for tests is adopted. The number in front of the name represents the dimension of the test. It is followed by two letters describing the presence of water in the tested sample: *Np* for non porous material,*Cd* for a porous material with a dry cluster, and *Po* for a porous material. The name is followed by a letter corresponding to the applied boundary condition: *D* as Dirichlet for imposed temperature, *N* as Neumann for imposed flux, and *S* as source. As an example, the first test we consider is a unidimensional non porous sample undergoing an imposed temperature; it is therfore refered to as 1NpD.

The chosen material is steel. Its parameters are given in Table 4.1.

Conductivity (W/mK)	14.6
Thermal expansion	1.10^{-5}
Young modulus (MPa)	2.10^{5}
Poisson's ratio (-)	0

Table 4.1 Parameters for steel

4.2 DIRICHLET BOUNDARY CONDITION

The initial temperature in the steel bar is $0^{o}C = 273.15K$. At the start of the computation, a constant temperature of $773.15K$ is applied on the top of the sample, yielding a difference of temperature $\Delta T = 500K$.

It takes 5.10^{6} s to reach the full steady state. To see the results in the transient state, a mid-time is defined. It is equal to 2.10^{6} s, i.e. the step 9 of the computations.

Figure 4.3 and Figure 4.4 show the distribution of temperature and heat flow along the bar at mid-time. The precise value of temperature at the bottom of the sample have to be determined precisely, but the qualitative results are satisfactory. Figure 4.5 presents the heat flux at steady state, when the heat field is constant along the bar. This flux can be neglected considering its maximum is 10^{-4} kNm/s. The computations made with a porous material with the bar set as a cluster dry give exactly the same results.

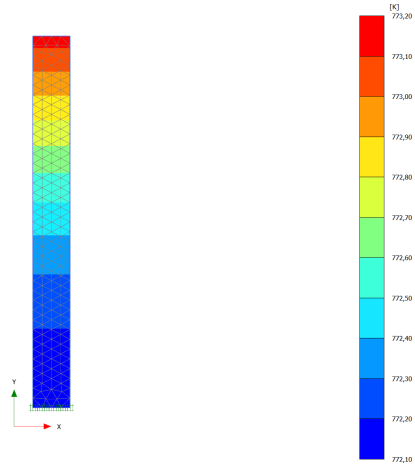

Figure 4.3 Distribution of temperature at mid time for 1NpD.

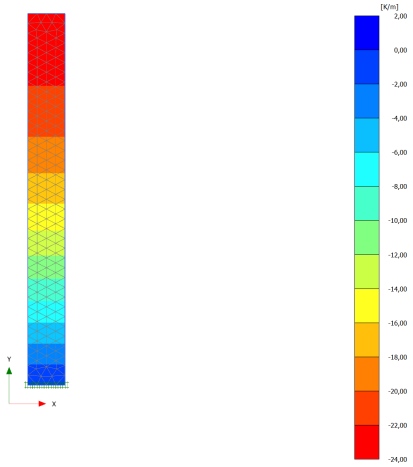

Figure 4.4 Vertical heat flow at mid time for 1NpD.

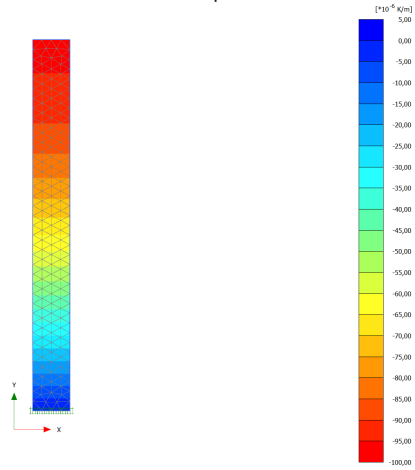

Figure 4.5 Vertical heat flow at steady state for 1NpD.

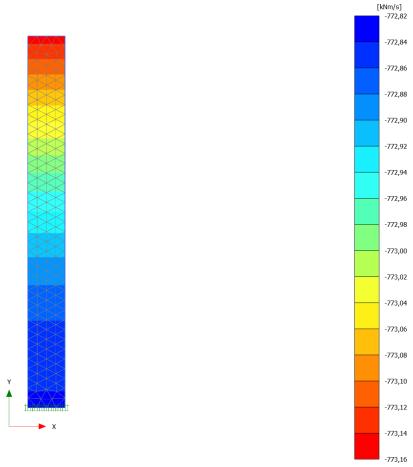

Figure 4.6 Vertical heat flow at mid time for 1NpN.

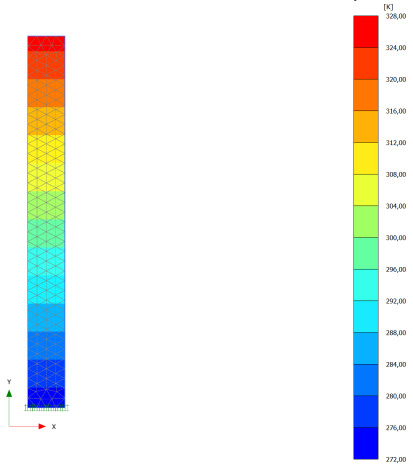

Figure 4.7 Distribution of temperature at steady state for 1NpN.

4.3 NEUMANN BOUNDARY CONDITION

The initial temperature in the bar is again set to 0^oC = 273.15K. At the start of the computation, a constant heat flow of 773.15 K/m is applied on the top of the sample. A Dirichlet BC has to be imposed on the bottom of the sample in order to cancel its zero flux default Neumann BC.

Figure 4.6 shows the flux at mid-time and Figure 4.7 shows the temperature when the flux has reached steady state. The temperature at the top of the bar is 326.1 K, which is equal to the analytical solution: $\Delta T = q_T \Delta X/\alpha$ = 326.1 K.

4.4 THERMAL EXPANSION

For the Dirichlet condition, the obtained thermal expansion corresponds to the expected value : $4.992.10^{-3}\ m \simeq \alpha \Delta T = 1.10^{-5} \times 500 = 5.10^{-3}\ m$.

For the Neumann condition, the obtained temperature on the top of the bar is 326.15 K, yielding ΔT = 53 K. The expected result is then $26.5.10^{-5}\ m$. The obtained value is $0.2648.10^{-3}\ m$, which is satisfactory.

5 VALIDATION: TWO-DIMENSIONAL HEAT FLOW AND STRUCTURAL ELEMENTS

The material used is the same as 1D: steel. The values of its parameters are given in table Table 4.1. The time parameters are the same as in the 1D section.

5.1 DIRICHLET BOUNDARY CONDITION

This type of condition is tested in three different ways: on the bottom of the sample, on its left side and on both bottom and left sides. In each case, a temperature of 773.15 K is applied in order to have a difference of temperature of 500 K.

BC only on bottom: In this section, a Dirichlet boundary condition is applied in the bottom of the sample. After 5.10^6 s, the steady state is reached. The resulting flow heat is negligible, even if displayed in the output. Figure 5.1 and Figure 5.2 present the temperature field and the resulting heat flux at mid-time.

BC only on left side: The conditons applied on the sample above are now applied on the left side of the sample. Figure 5.3 and Figure 5.4 present the temperature field and the resulting heat flux at mid-time. As expected, the temperature field and the heat flow are the same as above when rotating the sample with an angle of $-\pi/2$.

BC only on left side and bottom: The two preceding conditions are now applied on the left side of the sample on the bottom. Figure 5.5 presents the temperature field at mid-time. The temperature is increasing on the upper right corner, which is the expected behaviour. Additional similar figures taken at different times show the right propagation of heat, qualitatively.

Figure 5.6 presents the heat flow at mid-time. The high values on the lower right and the upper left corners may seem surprising. However, they represent show that heat is increasing in this diagonal direction as it is the place where the difference of temperature is the highest.

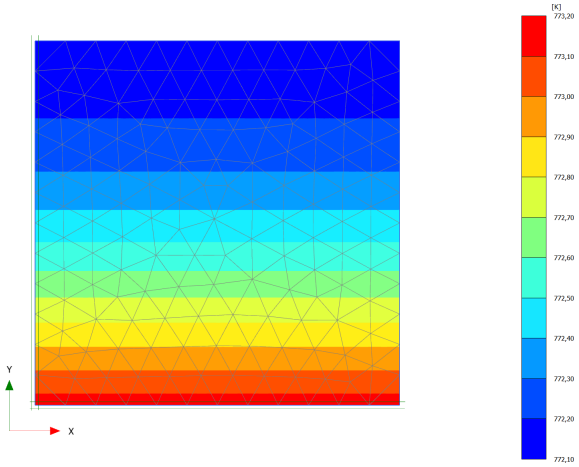

Figure 5.1 Temperature field at mid time for 2NpD, BC on the bottom.

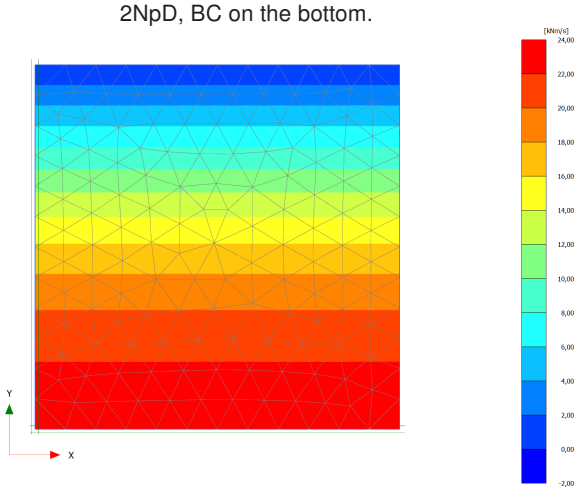

Figure 5.2 Heat flow at mid time for 2NpD, BC on the bottom.

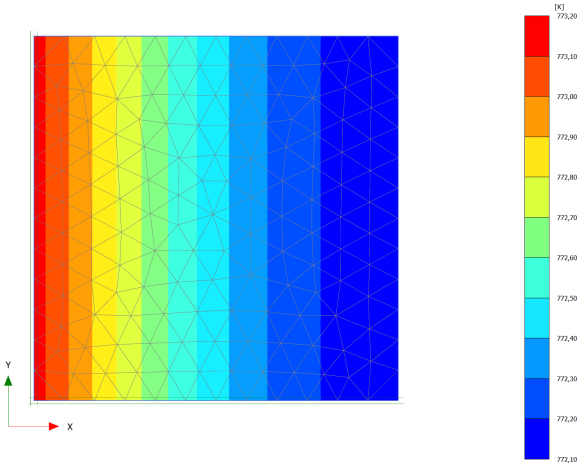

Figure 5.3 Temperature field at mid time for 2NpD, BC on the left.

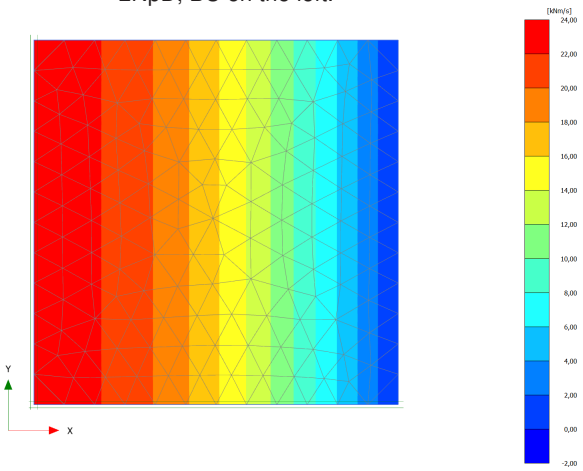

Figure 5.4 Heat flow at mid time for 2NpD, BC on the left.

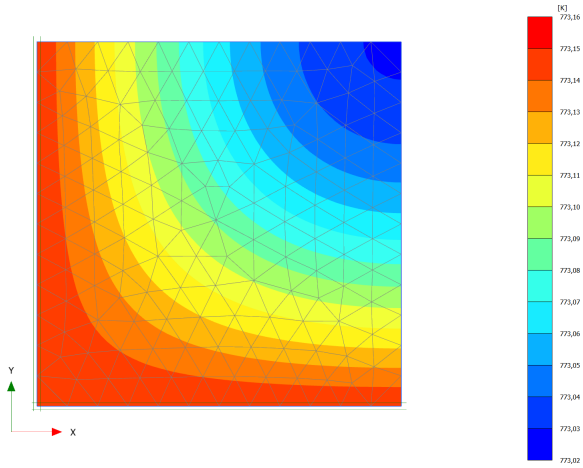

Figure 5.5 Temperature field at mid time for 2NpD, BC on both sides.

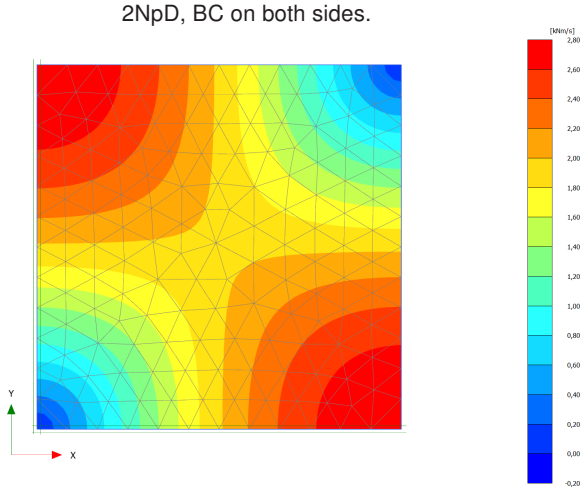

Figure 5.6 Heat flow at mid time for 2NpD, BC on both sides.

5.2 BEAM ELEMENTS

Four cases are taken into account:

1. One beam alone
2. Two beams
3. Horizontal beam with fixed displacements
4. Intersection of two beams

The interactions with the soil elements have not been taken into account. The geometry is made of a square sample of soil of 10m x 10m. The initial temperature is set to 20^{o}C. In cases 1, 2 and 4, a temperature of 60^{o}C is imposed at the top and at the bottom of the geometry, meaning a difference of temperature ΔT = 40^{o}C. This condition is applied to the left and right sides of the geometry in case 3. Four beams are defined, with the same material properties. Figure 5.7 shows the resulting geometry. The vertical beam chains are made of two aligned beams. The properties of the beams are given in Table 5.1. The weight of the beams has been set to zero in order to obtain a simple analytical result. Obtaining a steady-state solution requires 3.10^7 seconds, i.e. approximately one year (347 days).

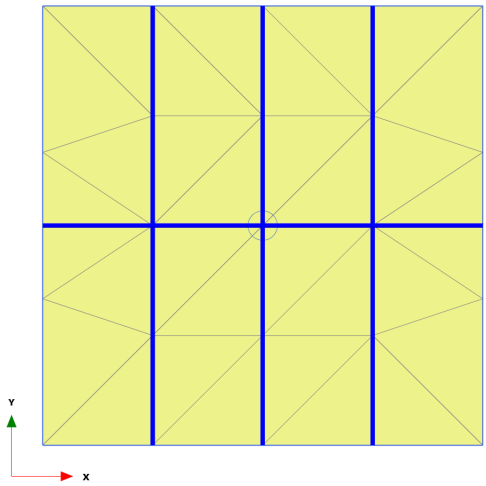

Figure 5.7 Geometry and mesh of the validation examples.

Volumetric mass ρ	Heat capacity c	Conductivity λ	Expansion α
7850 kg/m^3	450 J/Kkg	30 W/mK	5.10^{-5} m/mK
Equiv. thickness A	Young's modulus x thick. EA	Poisson's ratio ν	Weight w
0.3501 m	14.10^6 kN/m	0.15	0 $kN/m/m$

Table 5.1 Parameters used in the validations.

One beam alone: Figure 5.8 shows that the expected constant temperature field of 60^{o}C is obtained.

As $\varepsilon_T = \alpha \Delta T$, the expected thermal dilation is $\alpha \Delta T L = 5.10^{-5} \times 40 \times 10 = 0.02$, i.e. 2 cm, which is met exactly on Figure 5.9.

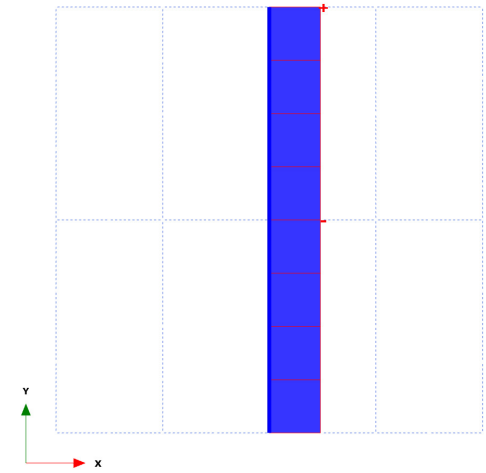

Figure 5.8 Temperature field for a single beam.

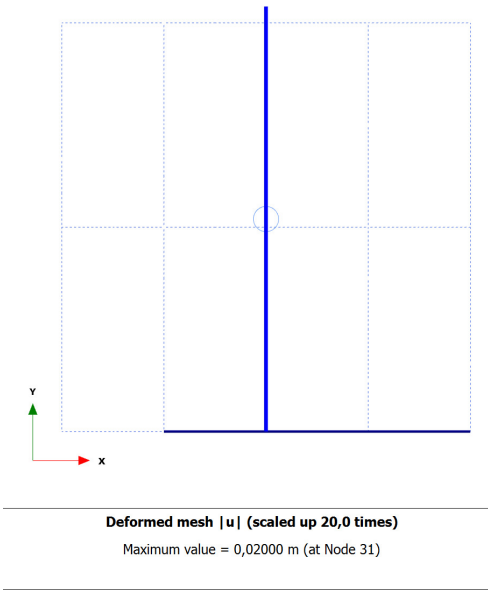

Figure 5.9 Thermal expansion for a single beam.

Two beams: This validation has for only ambition to show that the implementation is valid for more than one beam element and that provided the same boundary conditions, the temperature field and the thermal expansion are the same. Figure 5.10 shows that the thermal expansion of the two beams is equal. The same consistency for the temperature fields is found.

Horizontal beam with fixed displacements: In this validation, the horizontal beam shown in Figure 5.7 has fixed rotation and displacement on the left side, and fixed

displacement on the right side. As its weight is set to zero, no additional constraints on the right side are needed. A constant temperature of 60^oC is applied on both left and right sides.

The expected thermally induced normal force inside the beam is:

$$N = EA \cdot \varepsilon^T = EA \cdot \alpha \Delta T = 14.10^6 \cdot 5.10^{-5} \cdot 40 = 28.10^3 \, kN/m$$

The results shown in Figure 5.11 are slightly higher, about 2%, yet satisfactory.

Intersection of two beams: This section is more a verification than a validation; yet it demonstrates that the thermal beams integrate nicely with the current implementation of beams and hinges. The central vertical and the horizontal beams are connected together via a hinge, in order to allow the bending of the horizontal beam due to the thermal expansion of the vertical one. An imposed temperature of 60^oC is applied at the top and at the bottom of the domain. Figure 5.12 and Figure 5.13 show the resulting displacements and bending moments.

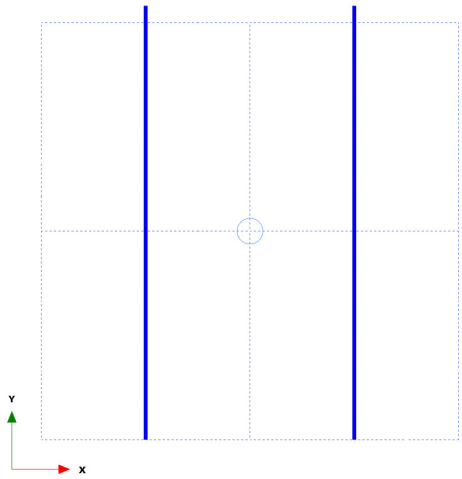

Deformed mesh |u| (scaled up 20,0 times)

Maximum value = 0,02000 m (at Node 35)

Figure 5.10 Thermal expansion of two equivalent beams.

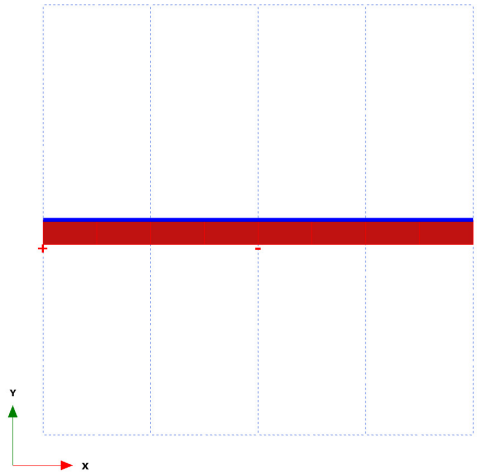

Axial forces N (scaled up $0{,}0200*10^{-3}$ times)

Maximum value = $-28{,}64*10^{3}$ kN/m (Element 9 at Node 2)

Minimum value = $-28{,}64*10^{3}$ kN/m (Element 10 at Node 48)

Figure 5.11 Thermally induced axial forces in a beam.

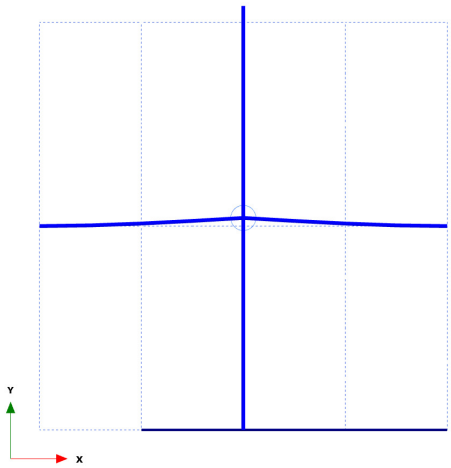

Deformed mesh |u| (scaled up 20,0 times)

Maximum value = 0,01997 m (at Node 31)

Figure 5.12 Thermal expansion and deformed mesh of two connected beams.

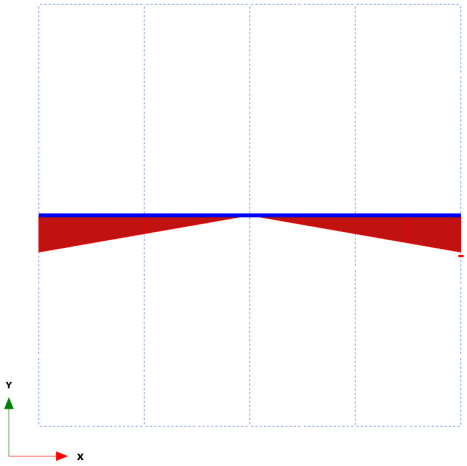

Bending moments M (scaled up 5,00*10^{-3} times)

Maximum value = -0,2446*10^{-12} kNm/m (Element 11 at Node 48)

Minimum value = -174,5 kNm/m (Element 12 at Node 57)

Figure 5.13 Resulting moments due to the thermal expansion of the joined vertical beam.

5.3 NODE TO NODE ANCHORS

The implementation for node-to-node anchors is based on the same pattern as beam elements. Their validation is however more limited as they cannot exist on their own: another type of element has to support them otherwise they are automatically disabled inside the kernel. We chose beam elements to support them. The geometry of the validation is shown at Figure 5.14.

As for the beam elements, the initial temperature in the domain is set to 20^{o}C. A prescribed temperature of 60^{o}C is applied to the top and the bottom of the sample. The thermal conductivity of the bearing beams is set to zero. The expected thermal expansion is also 2 cm, which is met on Figure 5.15.

This validation sums the specifications, as the correct thermal expansion implies a correct temperature field. Moreover, as the thermal expansion is calculated where the mechanical strains are calculated, the calculation of the forces inside the node-to-node anchor do take the effect of temperature automatically.

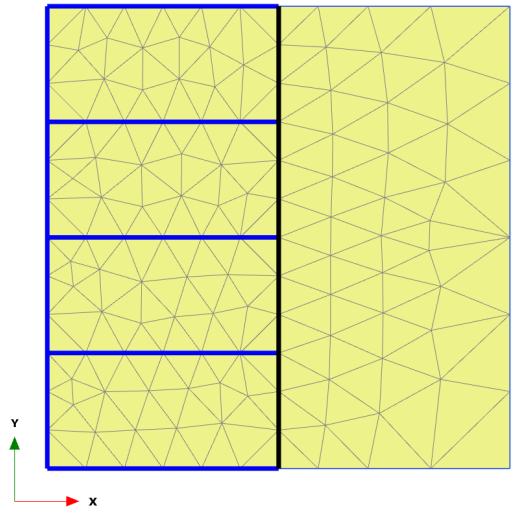

Figure 5.14 Geometry used to validate the node-to-node anchors.

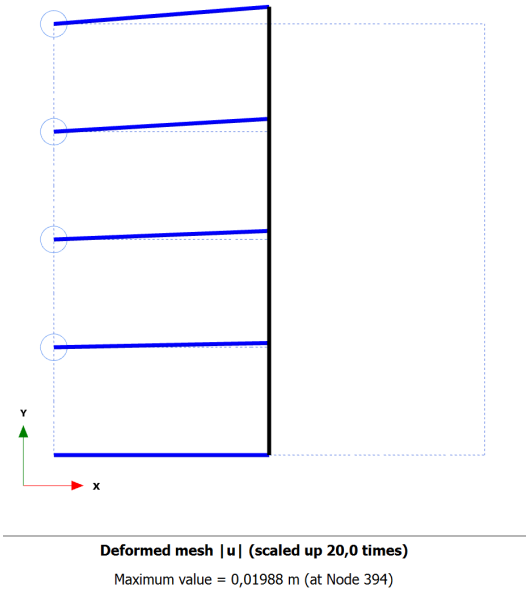

Figure 5.15 Resulting displacements due to the thermal expansion of the node-to-node anchors.

5.4 FIXED-END ANCHORS

Fixed-end anchors are used in case of a symmetry in a geometry. They are a simplified version of the node-to-node anchors. As they consist of just one node with node-to-node anchor material properties, only the thermal expansion needs to be implemented. More precisely, only the axial force resulting to the thermal expansion needs to be considered.

The validation relies then on the results of a classical excavation simulation using a

node-to-node anchor as a strut. Another analysis is performed using only the left part of the geometry and a fixed-end anchor, equivalent to the full case with the node-to-node anchor. The two geometries are shown on Figure 5.16 and Figure 5.17. The initial temperature is set to 20^oC. On the left and right sides, a temperature of 60^oC is imposed. The thermal properties of the soil and the beam elements are set to zero.

	N (kN/m)	N_{min} (kN/m)	N_{max} (kN/m)
NtN	-11.961	-11.961	1.201
FE	-11.915	-11.915	1.111

Table 5.2 Difference in results between node-to-node anchors (NtN) and fixed end anchors (FE) for the validation case.

	N (kN/m)	N_{min} (kN/m)	N_{max} (kN/m)
NtN	1.9	0	1.9
FE	1.77	0	1.77

Table 5.3 Difference in results between node-to-node anchors (NtN) and fixed end anchors (FE) without temperature.

Before presenting the results of the THM implementation of the fixed-end anchors, it is worth mentioning that the results for a standard consolidation TPP without temperature between the reference node-to-node anchor and the fixed-end anchor cases are less close than originally assumed, their difference about 7%, using the results presented in Table 5.3. The resulting displacements are presented in fig. Figure 5.18 and Figure 5.19, the forces in Table 5.2. The results between the reference and the fixed-end anchor cases are close enough to validate the implementation (less than a percent).

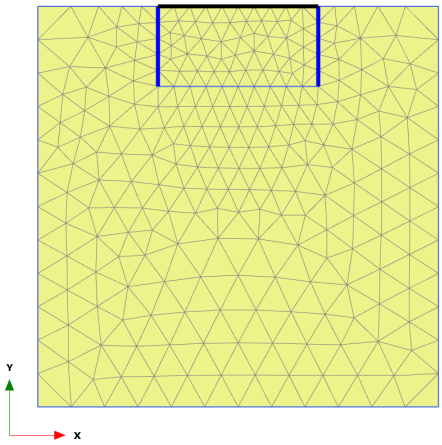

Figure 5.16 Reference geometry, 10m x 10m.

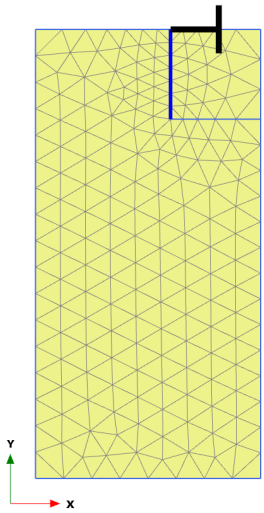

Figure 5.17 Geometry for the actual fixed-end anchor validation, 5m x 10m.

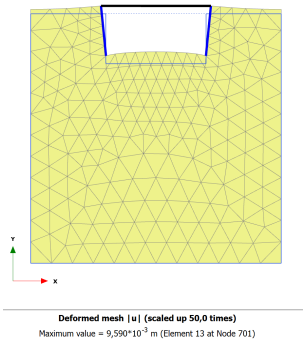

Figure 5.18 Resulting displacements for the reference case.

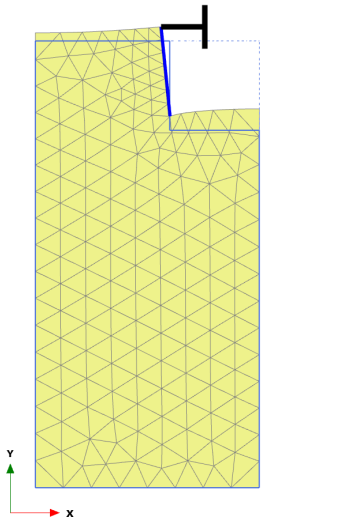

Figure 5.19 Resulting displacements for the fixed-end anchor calculation.

5.5 GEOTEXTILES

As for the node to node anchors, the geotextile elements cannot be validated on their own. If they are not laid on a soil layer, they are deactivated inside the kernel. The geometry used to validate the geotextiles is again a square of soil of 10m x 10m. A geotextile is created on the upper bound of the domain. Figure 5.20 shows the geometry of the study. The initial temperature in the domain is set to 20^{o}C. A temperature of 60 $^\circ C$ is applied on the left and right sides of the domain. The thermal expansion of the geotextile is set to 5. 10^{-5} K^{-1}, its ratio stiffness / area product is arbitrarily set to 10.

In this configuration, it is not possible to check the thermal expansion of the geotextile. Instead, the resulting axial force is checked, i.e. the left and right sides have horizontal fixities. The expected resulting force is:

$$F = \sigma A = \alpha \Delta T \,.\, EA = 5.10^{-5} \,.\, 40 \,.\, 10 = 0.02 kN/m$$

Figure 5.21 shows that the expected force is precisely reached, the negative sign showing the compression.

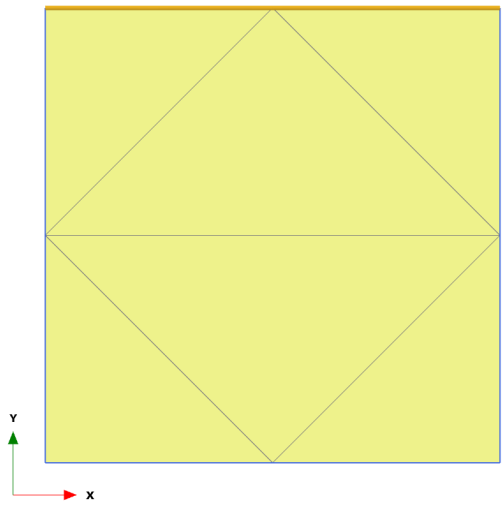

Figure 5.20 Geometry used to validate the geotextiles.

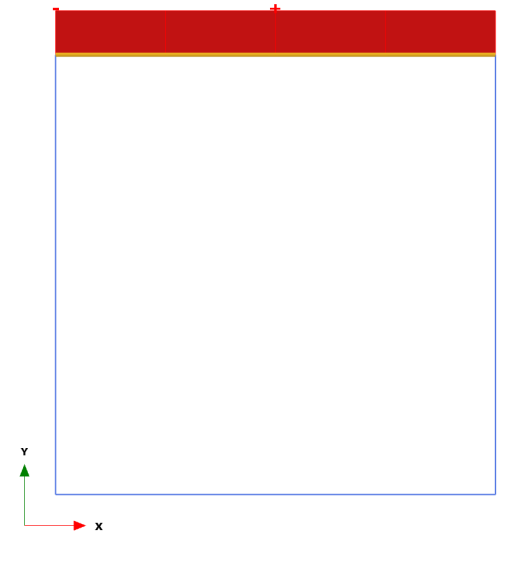

Figure 5.21 Resulting axial force due to the thermal expansion of geotextiles.

6 REFERENCES

[1] Brinkgreve, R.B.J., Engin, E., Swolfs, W. (2010). PLAXIS 2D, Finite element code for soil and rock analyses, users manual. PLAXIS B.V., The Netherlands.

[2] Galavi, V., Brinkgreve, R.B.J., Bonnier, P.G., Gonzalez, N.A. (2009). Fully coupled hydro-mechanical analysis of unsaturated soils. In Proceedings of Computational Geomechanics I, pp. 486-495.

[3] Khalili, N., Uchaipichat, A., Javadi, A.A. (2010). Skeletal themal expansion coefficient and thermo-hydro-mechanical cnstitutive relations for saturated homogeneous porous media. Mechanics of Materials, 42, 593–598.

[4] Martín, P.L., Barcala, J.M., Huertas, F. (2006). Large-scale and long-term coupled thermo-hydro-mechanic experiments with bentonite: the febex mock-up test. Journal of Iberian Geology, 32(2), 259–282.

[5] Romanovsky, V., Osterkamp, T. (2000). Effects of unfrozen water on heat and mass transport processes in the active layer and permafrost. Permafrost and Periglacial Processes, 11, 219–239.

[6] Rutqvist, J., Borgesson, L., Chijmatsu, M., Kobayashi, A., Jing, L., Nguyen, T.S., Noorishad, J., Tsang, C.F. (2001). Thermohydromechanics of partially saturated geological media: governing equations and formulation of four finite element models. International Journal of Rock Mechanics and Mining Sciences, 38, 105–127.

[7] Wang, W., Kosakowski, G., Kolditz, O. (2009). A parallel finite element scheme for thermo-hydro-mechanical (thm) coupled problems in porous media. Computers and Geosciences, 35, 1631–1641.